1-1-2014

Bright microwave pulses from PSR B0531+21 observed with a prototype transient survey receiver

J. Andrew O'Dea

F. A. Jenet

Tsan Huei Cheng

Chau M. Buu

Martin Beroiz

See next page for additional authors

Recommended Citation

J. Andrew O'Dea, et. al., (2014) Bright microwave pulses from PSR B0531+21 observed with a prototype transient survey receiver.Astronomical Journal147:5. DOI: http://doi.org/10.1088/0004-6256/147/5/100

The Astronomical Journal, 147:100 (8pp), 2014 May doi:10.1088/0004-6256/147/5/100

BRIGHT MICROWAVE PULSES FROM PSR B0531+21 OBSERVED WITH A PROTOTYPE TRANSIENT SURVEY RECEIVER

J. Andrew O'Dea[1], F. A. Jenet[2], Tsan-Huei Cheng[1], Chau M. Buu[1], Martin Beroiz[2], Sami W. Asmar[1], and J. W. Armstrong[1]
[1] Jet Propulsion Laboratory, California Institute of Technology, Pasadena, CA 91125, USA
[2] Department of Physics and Astronomy, University of Texas at Brownsville, Brownsville, TX 78520, USA
Received 2013 November 1; accepted 2014 February 1; published 2014 March 28

ABSTRACT

Recent discoveries of transient radio events have renewed interest in time-variable astrophysical phenomena. Many radio transient events are rare, requiring long observing times for reliable statistical study. The National Aeronautics and Space Administration/Jet Propulsion Laboratory's Deep Space Network (DSN) tracks spacecraft nearly continuously with 13 large-aperture, low system temperature radio antennas. During normal spacecraft operations, the DSN processes only a small fraction of the pre-detection bandwidth available from these antennas; any information in the remaining bandwidth, e.g., from an astronomical source in the same antenna beam as the spacecraft, is currently ignored. As a firmware modification to the standard DSN tracking receiver, we built a prototype receiver that could be used for astronomical transient surveys. Here, we demonstrate the receiver's utility through observations of bright pulses from the Crab pulsar and describe attributes of potential transient survey observations piggybacking on operational DSN tracks.

Key words: instrumentation: detectors – pulsars: individual (B0531+21)

1. INTRODUCTION

In the last ∼decade, observations of dynamic phenomena on timescales from nanoseconds to days or more (e.g., Hankins et al. 2003; Katz et al. 2003; Cordes et al. 2004; Kuniyoshi et al. 2003; Lorimer et al. 2007; Lazio et al. 2009; Burke-Spolaor & Bailes 2010; Macquart et al. 2010; Burke-Spolaor et al. 2011; Thornton et al. 2013) have renewed interest in transient radio phenomena and the astrophysics of their generation.

NASA's Deep Space Network (DSN) currently consists of 13 large-aperture, low-noise microwave tracking stations grouped in three complexes near Goldstone, California; Madrid, Spain; and Canberra, Australia. These stations are used almost continuously to track spacecrafts. In the course of normal operations, substantial bandwidth (e.g., 400 MHz at *X* band, ≈8.4 GHz) is transferred from the antenna front ends to signal processing centers at each tracking complex. However, only a small fraction of this bandwidth is processed for spacecraft tracking and telemetry; any information in the unused bandwidth—e.g., from an astronomical source in the same beam as the spacecraft—is ignored. Properly processed, this low-noise, high-sensitivity continuous tracking and wideband capability has value for studying the transient radio sky.

As a firmware change to the standard spacecraft tracking receiver, we built a prototype dispersion-correcting and transient-detecting receiver that processes information in the currently unexamined DSN bandwidth (Buu et al. 2011). This was a proof-of-concept instrument to demonstrate the feasibility of DSN piggyback astronomical observations without requiring any additional hardware. We report here observations of bright microwave pulses from PSR B0531+21 as an illustration of the capability and briefly describe the potential of astronomical observations piggybacking on operational DSN spacecraft tracks.

2. INSTRUMENT

Our receiver (dubbed "RRAT TRAP" for Rotating RAdio TransienT Receiver And Processor) implements a filter bank to correct impulsive signals for dispersion caused by propagation through the interstellar medium (ISM). The instrument is described by Buu et al. (2011).

The hardware platform for RRAT TRAP is the DSN's standard software-defined telecommunications receiver used to process spacecraft telemetry. The core of that receiver is a Xilinx Virtex-4 field-programmable gate array (FPGA). The DSN receiver is converted from operational use to filter bank/de-disperser/detector by modifying the start-up script to load different firmware into the FPGA and to run different software on the control computer. Because multiple telecommunications receivers are available at each DSN tracking complex, we can implement astronomical observations in a spare while normal DSN spacecraft tracking is done simultaneously with operational units.

The signal flow and on-instrument processing are described by Buu et al. (2011). Briefly, a radio signal is received at a DSN antenna and downconverted from *S* band (2.2–2.3 GHz), *X* band (8.2–8.6 GHz), or Ka band (31.8–32.3 GHz) to an intermediate frequency (IF). After downconversion, but in the signal path before the RRAT TRAP, an automatic gain control circuit (time constant ≈20 s) stabilizes the level of the IF signal. Using undersampling techniques and an anti-aliasing filter, the IF signal is digitized and downconverted to an 80 MHz digital bandwidth. (Although the prototype operates only over an 80 MHz bandwidth, the FPGA implementation could be scaled to the full front-end analog bandwidth if a different hardware platform were used.) The instrument processes this signal to produce detected power in a 64 channel filter bank over this 80 MHz band. Two time resolutions were implemented, 100 μs and 1 ms. In the 1 ms time resolution mode, RRAT TRAP does real-time de-dispersion/detection for 98 positive dispersion measure (DM) trials and 98 negative (non-physical) trials to search up to a maximum |DM| of 2000 cm^{-3} pc (Buu et al. 2011). At this time resolution the prototype's data buffering and disk writes keep up with real time. In the 100 μs resolution mode, which was used in testing for low to moderate DM pulsars including the B0531+21 observations reported here,

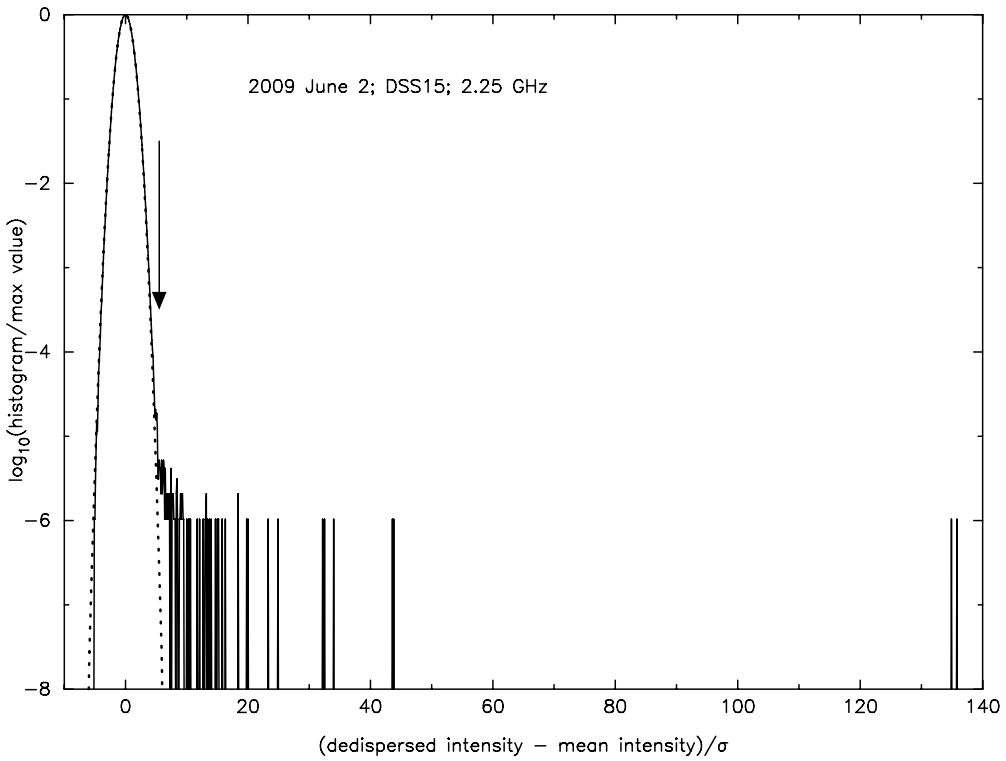

Figure 1. Histogram of ≈2.42 × 10^7 on-source de-dispersed data values at a 100 μs output rate. The standard deviation, $\sigma \approx 2.8$ K, corresponds to $T_{\rm sys} \approx 198$ K and is dominated by the noise temperature contribution from the Nebula, as discussed in the text. The dotted black line is a Gaussian with zero mean and unit variance; this accurately models the histogram to S/N ≈ 4, where an excess event rate occurs. Over this many trials, we expect fewer than one noise-only false alarm if the detection threshold for individually identifiable events is set at S/N = 5.5 (vertical arrow).

the data were buffered on the prototype for 5.2428 s and then written to the disk. Unfortunately, competition for resources from other running processes caused an unpredictable delay when offloading data to the disk and thus resulted in a non-unity duty cycle. This means the prototype could not keep track of the pulse phase from buffer to buffer at the 100 μs resolution.

3. OBSERVATIONS AND ANALYSIS

As part of field testing we observed several pulsars—in particular the Crab pulsar (e.g., Cordes et al. 2004; Jessner et al. 2005; Hankins & Eilek 2007; Karuppusamy et al. 2010; Majid et al. 2011)—from which we expected strong pulses from objects with a known DM. The observations were made on 2009 June 2 using DSS15, a 34 m antenna within the Goldstone, CA, DSN complex. We observed in circular polarization at *S* band (center frequency = 2.25 GHz) in two approximately equal-length sessions centered on 2145 UT and 2315 UT for a total on-source observing time of 2416.9 s. Between these two Crab pulsar observations, we took data on other objects including ≈530 s centered on 2205 UT pointed off-source (at the right ascension of the Crab but at declination 20.02 degrees). DSS15 at *S* band has gain of about 56.49 dB (Imbriale 2002), essentially independent of elevation for the high-elevation observations reported here, and an instrumental contribution to the system temperature of about 30 K. This gain corresponds to a sensitivity $\Gamma = (\lambda^2\ \text{gain})/(8\ \pi\ \text{k}) \approx 0.219$ K Jy^{-1}.

3.1. Crab Pulsar Observations

Radio maps made between 1.5–5 GHz show that the Crab Nebula's emission is enclosed in a region about 7′ × 7′. This is smaller than DSS15's *S*-band beam ($\approx\lambda/D = 13'$), so the Nebula is unresolved and the on-source system temperature, $T_{\rm sys}$, is dominated by the flux of the Nebula. The Nebula's flux, S_N, is modeled as 955 $(f/1\ \text{GHz})^{-0.27}$ Jy (e.g., Cordes et al. 2004). At 2.25 GHz, this gives $S_N \approx 767$ Jy and $T_{\rm sys}$, due to the average nebular flux and instrumental noise, of (767 Jy) Γ + 30 K ≈ 198 K. Our digital bandwidth is 80 MHz, but the 3 dB points of the anti-aliasing filter give an effective bandwidth for noise statistics, $B_{\rm eff}$, of about 50 MHz. The rms variation the system temperature measured off the bright pulses is $\Delta T_{\rm sys} = T_{\rm sys}/(B_{\rm eff}\tau)^{1/2} \approx 2.8$ K, where $\tau = 100\ \mu$s.

As noted above, the prototype stores the power in each of the 64 channels at 100 μs resolution in 5.2428 s chunks before writing to the disk. In post-processing we performed incoherent dispersion correction using the Crab's nominal DM (≈56.8 cm^{-3} pc) to produce a time series of dispersion-corrected data. Buu et al. (2011) show examples of dynamic spectra of strong individual pulses and time series of raw and de-dispersed pulses using our receiver (see also the Appendix for series of intensity along the dispersion track for our two brightest pulses). We estimated the rms noise away from any bright pulses in each buffer to normalize the de-dispersed data series as (de-dispersed intensity − mean intensity)/rms noise versus time.

The histogram of the ≈2.42×10^7 de-dispersed data values is shown in Figure 1. The dotted black line is a Gaussian with unit variance. A Gaussian accurately models the histogram out to S/N ≈ 4, where an excess positive count rate—the brighter pulses—occurs. To detect individual pulses reliably, we set the detection threshold to give less than one expected false alarm in 2.42×10^7 trials. We thus set the threshold for individual pulse detection at S/N = 5.5, which from the antenna gain and rms noise corresponds to 5.5 × 2.8 K/(0.219 K Jy^{-1}) ≈ 70.3 Jy ≈ 0.092 of the Nebula flux.

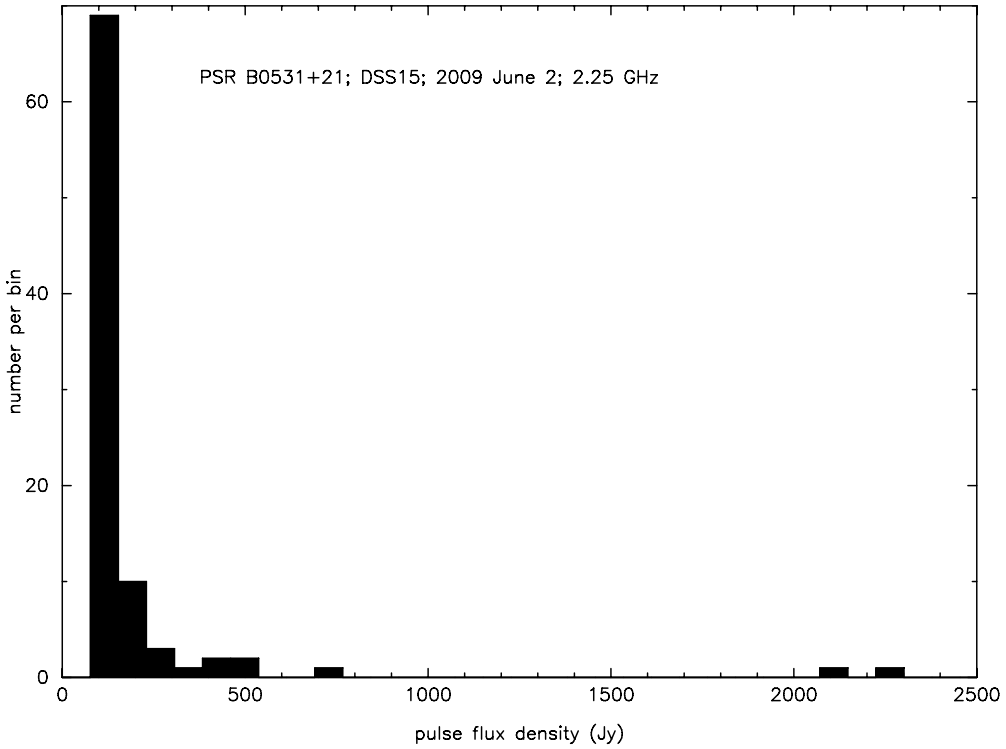

Figure 2. Histogram of estimated pulse fluxes for the 90 individually identified pulses in $T = 0.672$ hr of observation. Bin width is 10% of the estimated Nebula flux, with the exception of the lowest nonzero bin, which has width ≈10.9% of the estimated Nebula flux.

In $T \approx 0.672$ hr on-source, we observed 90 individually identified (S/N > 5.5) pulses. Of these, 74 were not time-resolved, i.e., were identified only in one 100 μs time slot; 13 spanned two contiguous time slots; and 3 spanned three contiguous time slots. A histogram of estimated pulse fluxes is shown in Figure 2. The largest pulses we observed have peak S/N ≈ 135 and estimated total flux densities ∼2000 Jy. Cordes et al. (2004), in a larger sample and with the Arecibo telescope, observed pulses with peak S/N ≈ 10^4 (at 430 MHz) and ≈10^3 (at 8.8 GHz). We note that *coherent* de-dispersion of wideband data shows sub-nanosecond structure and enormous flux density, ≈2,000,000 Jy, at microwave frequencies (Hankins & Eilek 2007).

Two pulses in our sample each had an estimated flux greater than that of the Nebula. This gives an apparent rate, r, for pulses brighter than the average Nebula $r \approx 3$ events hr^{-1}. Under assumptions we can extend this. If the rate of pulses brighter than the Nebula is viewed as a random variable having a Poisson distribution and with prior probability uniform over some (large) range, then Bayes' theorem (e.g., Gregory 2005) gives the probability density for the true rate, $\mathbf{r}$, given that $n = 2$ bright pulses were actually observed in time T: $p(\mathbf{r}|n) = T(\mathbf{r}T)^n e^{-\mathbf{r}T}/n!$. The 90% credible range for the true rate of S-band pulses brighter than the Nebula is then 1.2–9.4 events hr^{-1}.

3.2. Off-source Observations and Variable Assumed Dispersion Measure

We also took data off-source. With the Nebula out of the beam the system temperature dropped to ≈30 K, resulting in conditions more representative of potential piggyback DSN survey observations. As an assessment of data quality at this nominal $T_{\rm sys}$ and as a pilot blind search for short pulses at 100 μs resolution, we processed the off-source data varying the assumed DM. We searched 401 DM values in the range -1136 cm^{-3} pc ⩽ DM ⩽ +1136 cm^{-3} pc with granularity 5.68 cm^{-3} pc (i.e., 10% of the Crab's nominal DM). Processing with non-physical (negative) DMs is mainly intended to give a reference for noise-only statistics; however, if something were observed at negative DM—and if exotic radio frequency interference (RFI) could be excluded—it could be evidence for an intentional signal of extraterrestrial origin. Figures 3 and 4 show aggregate histograms of de-dispersed values for all zero and positive and all negative trial DMs, respectively.

With the exception of an outlier at S/N = 8.8 in Figure 3, the histograms are reasonably approximated as Gaussians with the expected variance. The outlier was a single event, ⩽100 μs in duration, observed in the DM = 0 processing channel. The excess pulse energy comes mainly from four contiguous channels (i.e., 5 MHz bandwidth) near the band center. This event is almost certainly terrestrial or near-Earth radio frequency interference which, at this low level, is de-dispersed to the skirts of the noise continuum when we process with the first nonzero trial DMs. We emphasize that the results shown in Figures 3 and 4 are based on only ≈530 s of data; we do not know if the near lack of impulsive S-band RFI would be typical in a more extensive survey at the Goldstone site.

4. SOME ATTRIBUTES OF TRANSIENT SURVEYS USING THE DEEP SPACE NETWORK

Figures of merit for transient searches involve waveform, survey speed, level of completeness, a priori probability of a source in the beam given the antenna pointing, and other considerations (e.g., Cordes 2007; Macquart 2011). But in any case one simultaneously desires a large effective solid angle and good sensitivity (to sense a large volume of space to the detection limit) and long observing time (to have a better chance of catching a rare event when it is "on"). Parkes

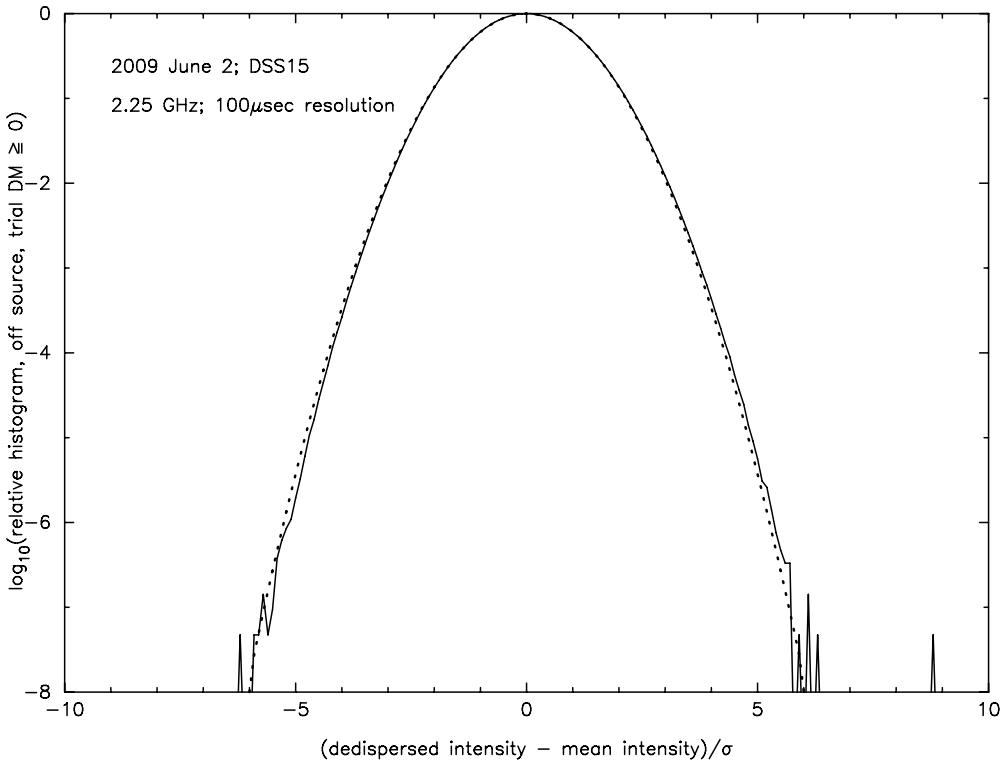

Figure 3. Histogram of $\approx 5.3 \times 10^6$ off-source data de-dispersed in post-processing with 201 trial zero and positive dispersion measures in the range $[0, +1136\ \mathrm{cm}^{-3}\ \mathrm{pc}]$. The standard deviation $\sigma \approx 0.42$ K for these off-source data corresponds to $T_{\mathrm{sys}} \approx 30$ K, as discussed in the text. The dotted black line is a Gaussian with zero mean and unit variance. The outlier at 8.8σ is a single 100 μs observation in the DM $= 0\ \mathrm{cm}^{-3}$ pc processing channel and is almost certainly low-level interference.

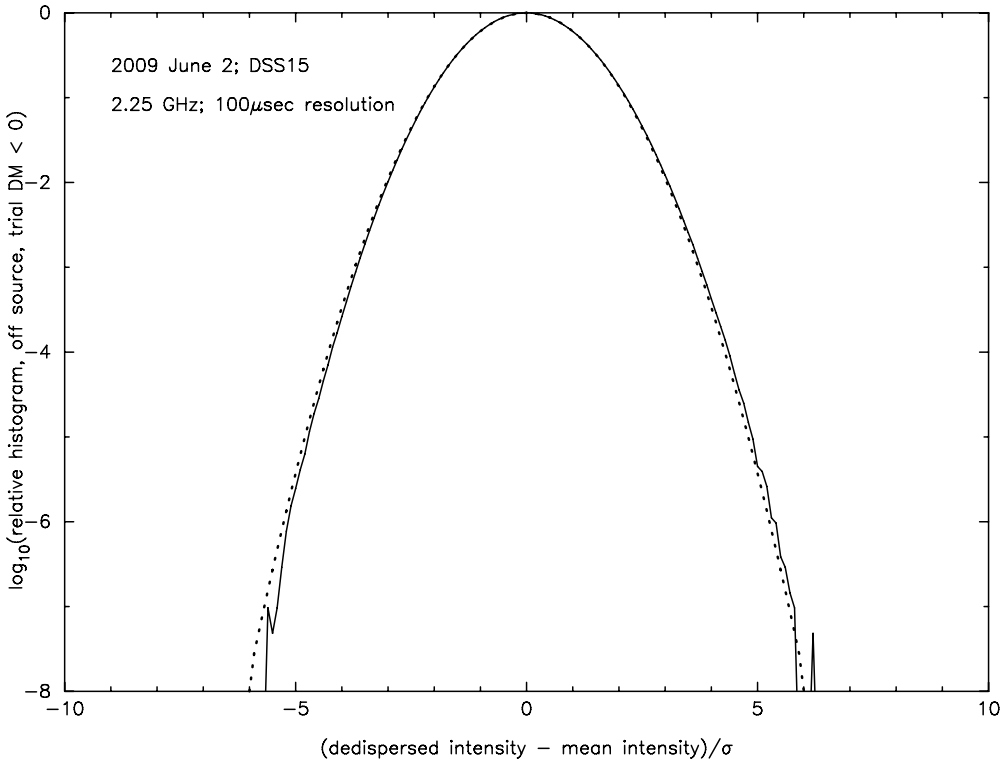

Figure 4. As in Figure 3, but with the off-source data processed with 200 trial negative dispersion measures in the range $(-1136\ \mathrm{cm}^{-3}\ \mathrm{pc}, -5.68\ \mathrm{cm}^{-3}\ \mathrm{pc})$. The standard deviation $\sigma \approx 0.42$ K for off-source data corresponds to $T_{\mathrm{sys}} \approx 30$ K. The dotted black line is a Gaussian with zero mean and unit variance.

archival data searches (e.g., Lorimer et al. 2007; Burke-Spolaor & Bailes 2010; Burke-Spolaor et al. 2011) have sensitivity similar to that of a DSN 70 meter antenna, and solid angle coverage comparable to a potential full DSN/RRAT TRAP implementation (due to Parkes multiple beam formation). The Fly's Eye search using the Allen Telescope Array uses multiple small telescopes to achieve a large solid angle (Siemion et al. 2010). The Pulsar ALFA survey (Cordes et al. 2006) used

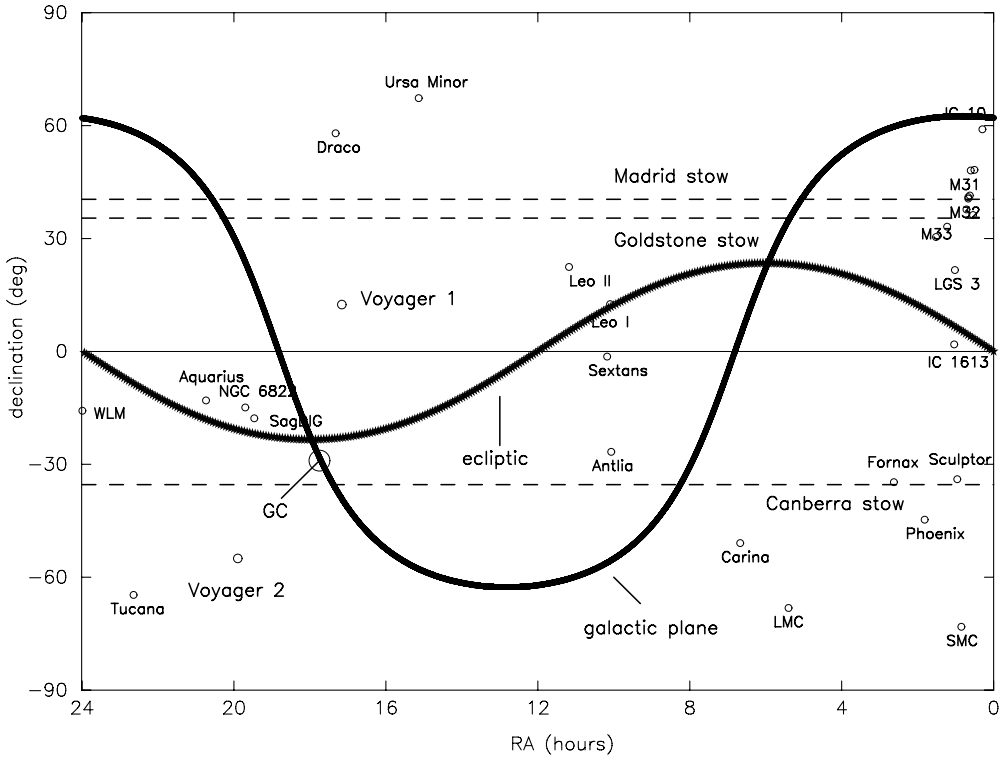

Figure 5. DSN sky coverage for potential astronomical surveys. The ecliptic and galactic planes are indicated; ≈80% of DSN observations are taken within a few degrees of the ecliptic. Dashed lines are the positions sampled when the antennas are at stow (for maintenance and for calibration intervals at the start and end of tracking passes; the antennas are pointed along these lines ≈10% of the time). Circles are some members of the Local Group of galaxies and the approximate angular positions of *Voyagers 1* and *2*. GC = galactic center.

multiple feeds to form 7 beams with the Arecibo telescope. PALFA thus had very good sensitivity (due to Arecibo's large collecting area) toward a region targeted to about ±5 degrees of galactic latitude near galactic longitudes ≈180 degrees and ≈50 degrees.

RRAT TRAP's novelty lies in its potential, without the necessity of additional hardware, to leverage the DSN's excellent microwave capability for long-term, good-sensitivity transient surveys. An implementation of a RRAT TRAP–like capability on all DSN tracks could substantially increase observing time for transient microwave phenomena (thus improving statistics for rare events) while looking mainly at the extragalactic sky. Targeted follow-up observations in the directions of candidate detections could be done at Goldstone with the DSN's research and development antenna (DSS13) or with radio astronomy antennas.

Piggyback DSN tracking would be astronomically untargeted. Figure 5 illustrates sky coverage for piggyback tracking. Most spacecraft tracked by the DSN are within a few degrees of the ecliptic plane; exact tracking depends on detailed network scheduling but we estimate 80% of antenna time (i.e., ≈0.8 × 8760 hr antenna^{-1} yr^{-1} × 13 antenna beams ≈91,000 beam hours yr^{-1}) are pointed within a few degrees of the ecliptic. Exceptions include tracking of a few non-ecliptic spacecraft (e.g., *Voyagers 1* and *2*), and vertical pointing at stow position during maintenance and during pre/post tracking pass calibrations (for perhaps 10% of the time each). When at stow, the sky is sampled along the three declination lines indicated, with the right ascension observed depending on the time of observation. One-tenth of the available time corresponds to about 11,400 beam hours yr^{-1} along these sky tracks. We estimate ≈17,000 beam hours yr^{-1} of tracking is within ±15 degrees of the galactic plane (mostly near right ascensions of 6 hr and 18 hr where the ecliptic crosses the galactic plane, with smaller contributions where the galactic plane is near the stow declinations of the DSN antennas).

In its perhaps most straightforward implementation, DSN piggyback tracks would, like RRAT TRAP, tap the IF signal at the point of the standard tracking receivers, i.e., after the ≈20 s time constant ACG. Although not a fundamental limitation, observing this way might simplify operations. Dedicated—versus firmware-repurposed, such as RRAT TRAP—hardware could use a different signal path and avoid this limitation while still capitalizing on the DSN microwave capability. A hardware development effort along these lines is underway at JPL for a dedicated "DSN Transient Observatory" (Kuiper et al. 2013). This instrument is designed to process multiple 500 MHz IF streams and could be used in this fashion.

5. CONCLUDING COMMENTS

We demonstrated that astronomical information can be extracted from available DSN tracking data bandwidth that is not currently being analyzed. This information can be obtained via firmware modifications to existing spacecraft tracking receivers, leveraging the DSN's microwave capabilities without the necessity of new hardware. Piggyback observations on standard DSN spacecraft tracks would allow astronomical survey observations for transient events—mostly near the ecliptic plane and thus mostly extragalactic—complementary to searches in targeted galactic directions.

The authors thank Ron Creech and Larry Bracamonte of ITT and the Goldstone team for supporting the test passes at

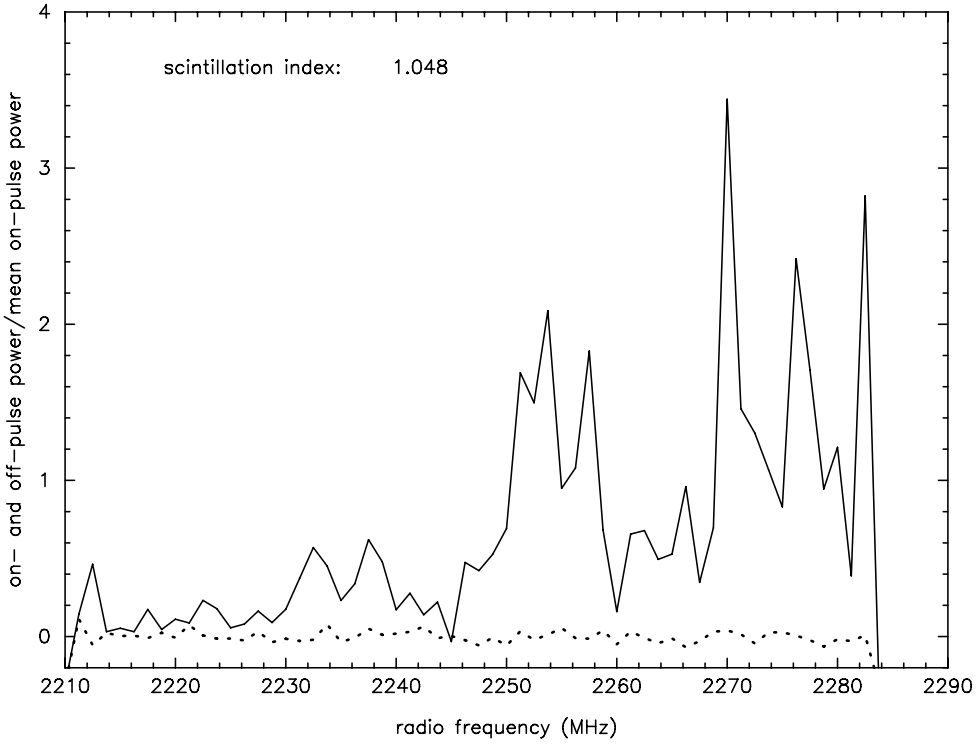

Figure 6. Plot of on- (solid) and off- (dotted) pulse intensity in a 100 μs wide strip along the Crab's nominal dispersion track, corrected for passband gain, as a function of radio frequency for the second brightest pulse observed.

DSS15. We benefited from discussions with W. A. Coles and Richard Woo. Development of the RRAT TRAP prototype was supported under the Director's Research and Development Fund at JPL. For the JPL authors, the research described here was carried out at the Jet Propulsion Laboratory, California Institute of Technology, under a contract with the National Aeronautics and Space Administration.

APPENDIX

SCINTILLATION

Here, we briefly discuss radio wave scintillation on our two brightest pulses and estimate turbulence levels required to produce the observed scintillation characteristics.

Our observations were made at a solar elongation angle of ≈12 degrees, sufficiently large that interplanetary intensity scintillation effects at *S* band (e.g., Coles 1978) are negligible.

The Crab pulsar displays both refractive and diffractive interstellar scintillation. For our 2.25 GHz observations, extrapolation of the data in Figure 3 of Rickett & Lyne (1990) suggests a refractive timescale of ∼12 hr, i.e., long compared to the span of our observations. Thus, our data set is probably homogeneous with respect to refractive intensity variations.

We expect scattering from both the general ISM and locally from the Nebula. The strength of the scintillation is characterized by $U =$ the square of the Born approximation to the intensity scintillation index (scintillation index, $m =$ rms intensity/mean intensity). If $U \gg 1$, the scintillations are strong and the scintillation theory predicts $m = 1$ (Rumsey 1975). Although specific situations are clearly more complicated (e.g., Higdon 1984, 1986; Fiedler et al. 1987; Brisken et al. 2010), interstellar scintillations are often interpreted in terms of scattering from isotropic, statistically stationary turbulence. Assume an isotropic Kolmogorov spectrum of ISM electron density fluctuations, spectral level $C_n^2 = 0.001\ \mathrm{m}^{-6.67}$ (Armstrong et al. 1995), and an Earth–pulsar distance $z = 2$ kpc. Equation (38) of Rickett (1977) relates U to the turbulence level and propagation distance: $U = 8\,\pi^2\,r_e^2\,\lambda^2\,C_n^2\,z^{(\alpha/2)}\,(\lambda/2\pi)^{(\alpha-2)/2}\,\sin(\pi\alpha/4)\,\Gamma(2-\alpha/2)\,\Gamma(\alpha/2)^2/(\alpha-2)\,\Gamma(\alpha)$, where r_e is the classical electron radius, λ is the radio wavelength, and $\alpha = 11/3$ for Kolmogorov turbulence. This predicts $U \approx 10^3$ for our *S*-band observations. The decorrelation bandwidth ($\Delta\nu =$ half-width to 1/e of the radio frequency autocorrelation function) can be estimated from Equation (41) of Rickett (1977); we compute $\Delta\nu \approx 3$ MHz, again with $C_n^2 = 0.001\ \mathrm{m}^{-6.67}$ and $z = 2$ kpc.

Previous observations of giant pulses from the Crab near our observing frequency (e.g., Cordes et al. 2004) show clear intensity modulation over frequency intervals much smaller than our total 80 MHz bandwidth. Cordes et al. (2004) determined $\Delta\nu = 2.3 \pm 0.4$ MHz at 2.33 GHz. Figures 6 and 7 show intensity versus frequency measured in the 100 μs wide strips along the Crab's nominal dispersion track in (time, radio frequency), giving peak signal-to-noise ratio (S/N) for our two brightest pulses. Additionally, shown in each plot is a reference "off-pulse" intensity versus frequency measured along the same dispersion track, but offset in time 500 μs earlier than the bright pulses. We have corrected both on- and off-pulse intensity series for non-uniform passband gain by dividing by the average gain at each frequency channel and, for this analysis, have omitted the five highest frequency channels and the single lowest frequency channel because of very low gain near the band edges. The series show deep fades—to the noise level—as expected/required if $U \gg 1$. We estimate the intensity scintillation index, m, for these two series to be 1.108 and 1.048. These are probably consistent with unity, as expected for strong scintillation, given the small number of independent samples going into each estimate. The decorrelation bandwidth (estimated from the average of the sample autocorrelations of the two pulses in Figures 6 and 7) is $\mathrm{HWe}^{-1} \approx 5.5$ MHz. (Bounds for the decorrelation bandwidth

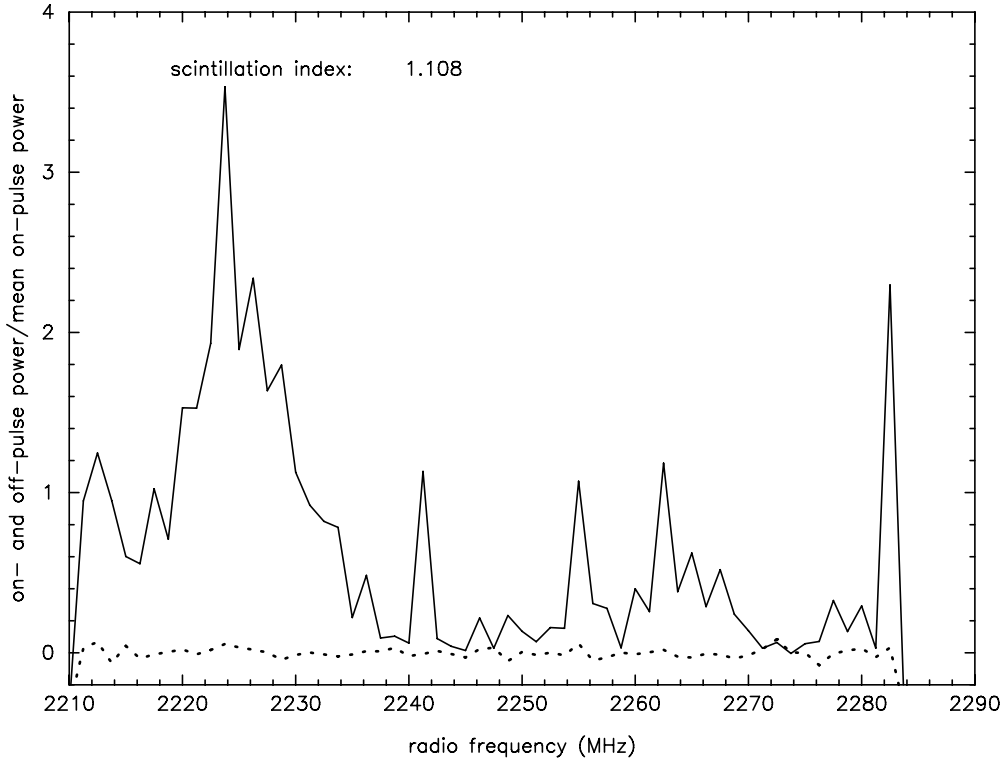

Figure 7. As in Figure 6, but for the brightest pulse observed.

also come immediately from the observation that $m \approx 1$. $\Delta\nu$ must be greater than our per-channel bandwidth, 1.25 MHz, or else the observed scintillation index would be suppressed due to averaging of fluctuations within each channel. $\Delta\nu$ must also be small compared with our full 80 MHz bandwidth; if it were not, the scintillation would cause the whole band to brighten and dim simultaneously, resulting in an empirically determined scintillation index—estimated over this finite bandwidth—to be less than unity. That is, $m \approx 1$ by itself means 1.25 MHz $< \Delta\nu \lesssim$ 8 MHz.)

Our data make only a weak statement about the diffractive timescale, $\Delta\tau_D$. Scintillations in the two pulses in Figures 6 and 7 manifest themselves in different parts of the band in the $\approx$16.8 minute time separation between these two pulses. Thus, $\Delta\tau_D$ is plausibly <16.8 minutes. We note that Cordes et al. (2004), observing at 2.33 GHz, estimated 35 $\pm$ 5 s from more extensive observations.

The computed decorrelation bandwidth, using a plausible general ISM turbulence level and known distance to the pulsar, roughly agrees with our observation. However, Karuppusamy et al. (2010), from order-of-magnitude variability of single pulse scattering within a 6 hr observation, conclude that most of the scattering cannot be due to the general ISM and that the bulk of the scintillation must arise from within the Nebula itself. If the scattering causing a decorrelation bandwidth of $\approx$5.5 MHz comes from a thin screen within the Nebula, we can bound the strength of turbulence required. A direct and a scattered ray will exhibit a time difference, Δt, due to their separate paths $\approx 1/(2\pi\Delta\nu) \approx 29$ ns. The scattering angle required to achieve this depends on the location of the screen within the Nebula. The minimum scattering angle ϕ giving a 29 ns path delay difference is $\approx 2 \times 10^{-8}$ radians, which occurs for a screen at the edge of the Nebula. From the scattering angle we can determine the phase coherence length at the exit plane of the screen: $\phi \sim \lambda/b_{\rm coh}$, where $b_{\rm coh}$, the coherence scale, is the transverse distance over which the phase structure function is 1 rad^2. The phase structure function can then be related to the turbulence level, C_n^2, and the propagation distance, z, via, e.g., Equation (3) of Armstrong et al. (1995). For $\phi \gtrsim 2 \times 10^{-8}$ radians, the $C_n^2\, z$ product is constrained to be $\gtrsim 2 \times 10^{18}$ m$^{-5.67}$. This value can be compared, e.g., to the $C_n^2\, z$ product for interplanetary scintillation in the antisolar direction inferred from meter-wavelength intensity scintillation: $\sim 4 \times 10^{15}$ m$^{-5.67}$.

From an assumed screen thickness we can infer a lower bound to the turbulence level from the bound on the $C_n^2\, z$ product. If the screen thickness were comparable to the width of a Nebula filament ($\sim 6 \times 10^{14}$ m) then C_n^2 would be $\gtrsim 3 \times 10^3$ m$^{-6.67}$. Very long baseline interferometry/scintillation observations of anisotropic irregularities in the ISM (Brisken et al. 2010) show filamentary structures with dimensions as small as $\sim 10^{10}$ m; such a screen thickness would give $C_n^2 \gtrsim 2 \times 10^8$ m$^{-6.67}$. These are 6–11 orders of magnitude larger than the electron density turbulence level usually ascribed to the general ISM.

REFERENCES

Armstrong, J. W., Rickett, B. J., & Spangler, S. R. 1995, ApJ, 443, 209
Brisken, W. F., Macquart, J.-P., Gao, J. J., et al. 2010, ApJ, 708, 232
Burke-Spolaor, S., & Bailes, M. 2010, MNRAS, 402, 855
Burke-Spolaor, S., Bailes, M., Johnston, S., et al. 2011, MNRAS, 416, 2465
Buu, C. M., Jenet, F. A., Armstrong, J. W., et al. 2011, Proc. IEEE, 99, 889
Coles, W. A. 1978, SSRv, 21, 411
Cordes, J. M. 2007, SKA Memorandum 97, http://www.skatelescope.org/uploaded/55809_97_memo_Cordes.pdf
Cordes, J. M., Bhat, N. D. R., Hankins, T. H., McLaughlin, M. A., & Kern, J. 2004, ApJ, 612, 375
Cordes, J. M., Freire, P. C. C., Lorimer, D. R., et al. 2004, ApJ, 637, 446
Fiedler, R., Dennison, B., Johnston, K. J., & Hewish, A. 1987, Natur, 326, 675
Gregory, P. 2005, Bayesian Logical Data Analysis for the Physical Sciences (Cambridge: Cambridge Univ. Press)

Hankins, T. H., & Eilek, J. A. 2007, ApJ, 670, 693
Hankins, T. H., Kern, J. S., Weatherall, J. C., & Eilek, J. A. 2003, Natur, 422, 141
Higdon, J. 1984, ApJ, 285, 109
Higdon, J. 1986, ApJ, 309, 342
Imbriale, W. A. 2002, Deep-Space Communications and Navigation Series, Monograph 4 (JPL Publication 02-6; Pasadena, CA: California Institute of Technology)
Jessner, A., Slowikowska, A., Klein, B., et al. 2005, AdSpR, 35, 1166
Karuppusamy, R., Stappers, B. W., & van Straten, W. 2010, A&A, 515, A36
Katz, C. A., Hewitt, J. N., Corey, B. E., & Moore, C. B. 2003, PASP, 115, 675
Kuiper, T. B., Lazio, T. J., Majid, W. A., et al. 2013, DSN Transient Observatory, Poster 439.14, 221st American Astronomical Society Meeting, https://aas.org/files/resources/aas_221_abstracts.pdf
Kuniyoshi, M., Matsumura, N., Takefuji, K., et al. 2007, PASP, 119, 122
Lazio, J., Bloom, J. S., Bower, G. C., et al. 2009, The Dynamic Radio Sky: An Opportunity for Discovery, Science White Papers, No. 176 (arXiv:0904.0633v1)
Lorimer, D., Bailes, M., McLaughlin, M. A., Narkevic, D. J., & Crawford, F. 2007, Sci, 318, 777
Marquart, J.-P. 2011, ApJ, 734, 20
Macquart, J.-P., Bailes, M., Bhat, N. D. R., et al. 2010, PASA, 17, 272
Majid, W. A., Naudet, C. J., Lowe, S. T., & Kuiper, T. B. H. 2011, ApJ, 741, 53
Rickett, B. J. 1977, ARA&A, 15, 479
Rickett, B. J., & Lyne, A. G. 1990, MNRAS, 244, 68
Rumsey, V. 1975, RaSc, 10, 107
Siemion, A., Von Korff, J., McMahon, P., et al. 2010, AcA, 67, 1342
Thornton, D., Stappers, B., Bailes, M., et al. 2013, Sci, 341, 53